Influence of Nanotube Length on the Optical and Conductivity Properties of Thin Single-Wall Carbon Nanotube Networks

Daneesh Simien, Jeffrey A. Fagan, Wei Luo, Jack F. Douglas, Kalman Migler, and Jan Obrzut*

Polymers Division, National Institute of Standards and Technology, Gaithersburg, Maryland 20899

ABSTRACT We study the optical and electrical properties of transparent conducting films made from length-sorted single-wall carbon nanotubes (SWCNT). Thin films of length-sorted SWCNTs, formed through filtration from a dispersing solvent onto a filter substrate ("buckypaper"), exhibit sharp changes in their optical properties and conductivity (σ) with increasing SWCNT surface concentration. At a given surface concentration, tubes longer than 200 nm are found to form networks that are more transparent and conducting. We show that changes of σ with SWCNT concentration can be *quantitatively* described by the generalized effective medium (GEM) theory. The scaling universal exponents describing the "percolation" transition from an insulating to a conducting state with increasing concentration are consistent with the two-dimensional (2D) percolation model. Shorter tubes and mixed length tubes form 3D networks. Furthermore, we demonstrate that the conductivity percolation threshold (x_c) varies with the aspect ratio L as, $x_c \sim 1/L$, a result that is also in accordance with the percolation theory. These findings provide a framework for engineering the optical and electrical properties of SWCNT networks for technological applications where flexibility, transparency, and conductivity are required.

KEYWORDS: carbon nanotubes · buckypaper · percolation · 2D networks · conductivity · optical properties

Thin films of carbon nanotubes (CNT) have been studied as viable semiconductors,[1] chemical sensors,[2,3] and transparent conductive coatings.[4,5] The attractive feature of these materials is that the addition of a relatively small amount of nanotubes can have a profound influence on the conductivity, optical, and mechanical properties. The conductivity percolation threshold is the critical concentration where the conductivity of the networks changes dramatically. Because of their high aspect ratio, carbon nanotube networks have one of the smallest percolation thresholds among known materials. The percolation threshold of these network scales inversely to the aspect ratio of the CNTs. Thus, percolation can occur at concentrations of CNTs of much less than 1% by volume or area in three and two dimensions, respectively. Attractive electronic properties of single-walled carbon nanotubes (SWCNT) motivate the development of field-effect transistor configurations with the SWCNT films as an active channel material. In these efforts, the channel length is typically comparable to tube length,[6,7] and thus a small number of tubes renders the whole network conducting. Networks with a randomized orientation of nanotubes show higher conductivities than those made of perfectly aligned tubes.[8,9] Near the percolation threshold, the conductivity exhibits a power law dependence on the network geometrical parameters, but the values of the critical exponents are nonuniversal. Rather, they are dependent upon the geometrical configuration of the device.[9] Moreover, the length distribution of the CNTs used is generally broad and often poorly characterized. Consequently, these configurations, while interesting, do not comply with the classical percolation model. This makes it difficult to develop an understanding of the phenomena that control the overall optical and electrical properties of thin carbon nanotube networks, which presents a challenge in the design of new materials for transparent electronics and other applications.

Here, we investigate the electrical conductivity and optical transparency percolation transitions as a function of the length of carefully fractionated and purified SWCNTs[10,11] in layers that are thin enough to be idealized as two-dimensional (2D) networks. These percolation transitions are contrasted with those in polydisperse SWCNT layers that we find are better described as three-dimensional (3D) SWCNT networks. Our theoretical description of the conductivity and optical percolation of SWCNT networks relies on generalized effective medium (GEM) theory,[12] which

*Address correspondence to jan.obrzut@nist.gov.

Received for review June 16, 2008 and accepted August 20, 2008.

Published online September 9, 2008.
10.1021/nn800376x CCC: $40.75

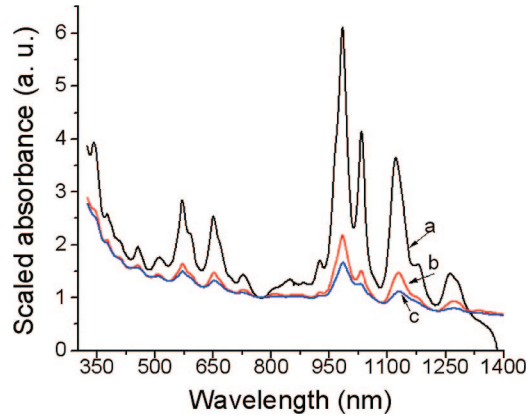

Figure 1. Optical absorbance spectra of length-sorted SWCNT in aqueous suspensions for the following tube lengths and concentration: (a) 820 nm, 0.0078 mg/mL; (b) 210 nm, 0.036 mg/mL; and (c) 130 nm, 0.1125 mg/mL.

combines the features of percolation theory and the effective medium theory without assuming an infinite property contrast between the additive and the matrix material. In a previous paper, we applied the GEM theoretical framework to describe polymer nanocomposites of multiwall carbon nanotubes and polypropylene subjected to steady shear.[13] In the present paper, we show that GEM theory continues to perform well when applied to quasi two-dimensional carbon nanotube films. We anticipate that this type of characterization of property change in buckypaper layers will aid in the design of new materials for developing transparent electronics and other applications.

RESULTS AND DISCUSSION

Our materials (buckypaper) are made from well-dispersed aqueous suspensions of length-sorted SWCNTs *via* a vacuum filtration onto nanoporous membranes. Figure 1 shows absorbance spectra of SWCNTs in liquid suspensions normalized to the baseline π-plasmon absorbance at 775 nm.

The mean lengths of the fractions used were 820, 210, and 130 nm. In the spectra, the absorption bands at 850−1450 nm and at 500−850 nm are due to E_{11}^{s} and E_{22}^{s} interband electronic transitions in semiconducting tubes;[14] the absorption bands between 420 and 520 nm are due to electronic transitions in metallic tubes E_{11}^{m}, while the 340−400 nm band corresponds to the $E33^{s}$ transition in semiconducting tubes.[14−17] The longer tubes display stronger electronic transitions, allowing for the projection of the average SWCNT length.[11] The spectra indicate that the chirality distribution is nearly equivalent in all samples, where ≈1/3 are metallic.[4,16,17] Raman scattering studies performed on the length-sorted fractions of SWCNT indicated that these fractions represent a low level of defects. The ratio of the D to G band intensities was about 0.02 for fractions above 200 nm and decreased with increasing SWCNT length, consistent with the end cap effect. This illustrates that the D band, often associated with defect

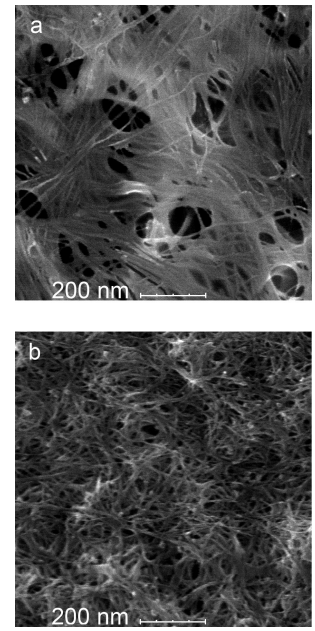

Figure 2. Scanning electron microscope images of SWCNT films for the following tube lengths and surface densities: (a) 820 nm, 0.02 μg/cm^2; and (b) mixed length, 1.4 μg/cm^2.

density, was negligibly small for these length-sorted fractions.[17]

The SEM image shown in Figure 2a is representative of a 2D network of nanotubes having a mean length of 820 nm. The network is near the percolation threshold, when surface density is about 0.02 μg/cm^2 (see below). The connectivity length seen in Figure 2a is about 500 nm. The nanotubes do not exhibit excessive bundling or reagglomeration upon deposition and rinse removal of surfactant as deposited on the surface of the membrane. The SWCNTs make a continuous network in spite of areas where membrane pores are observed. In Figure 2b, the mixed length tubes form a three-dimensional network. The surface density of these mixed length tubes is about 1.4 μg/cm^2, which is well above the percolation threshold.

The optical properties of the thin SWCNT film samples were evaluated by measuring a combination of reflectance and absorbance using a diffuse reflectance accessory kit on our spectrophotometer. This procedure allowed us to determine the optical characteristic directly without transferring the film onto a transparent substrate, while preserving the random structure of the network formed during the vacuum filtration process. The spectra in Figure 3 are shown for selected SWCNT solid films for unsorted samples and for fraction lengths of 130, 210, and 820 nm. The spectra are referenced to the reflectance of the membrane without the tubes and, therefore, correspond directly to the transmittance (T) of the SWCNT films. These SWCNT films are about 20 nm thick, approaching a conductivity plateau above the percolation threshold, while their transparency is about 85−90% at the wavelength of 775 nm. The absorption peaks that appear in the NIR

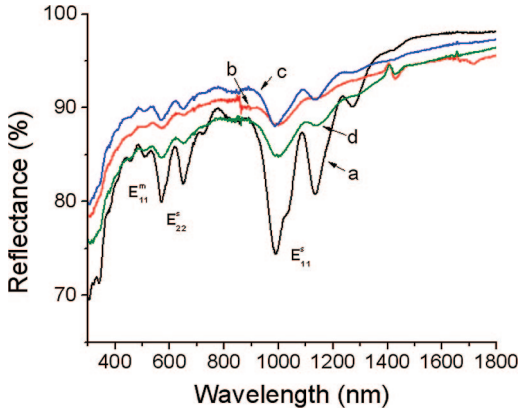

Figure 3. Optical reflectance of SWCNT networks for the following tube lengths and surface densities: (a) 820 nm, 0.434 μg/cm^2; (b) 210 nm, 0.517 μg/cm^2; (c) 130 nm, 0.564 μg/cm^2; and (d) mixed length tubes, 0.455 μg/cm^2.

and in the visible range of the spectrum are characteristic of specific tube chiralities. E^s_{11} and E^s_{22} are due to electronic interband transitions rising from semiconducting tubes, while E^m_{11} are electronic transitions from metallic tubes, which are similar to those shown in Figure 1 for the length-sorted nanotubes in liquid suspension. The absorption features, E^m_{11}, attributed to the metallic chirality is estimated to comprise about 30% of the sample. We note that the normalized intensities of the absorption peaks in the films are lower than those in suspensions shown in Figure 1 for the corresponding tube length. The effect of decreasing intensity of the characteristic electronic transitions in the network is likely due to interactions between interconnecting tubes. Diminished absorbance intensities can likewise be attributed to doping by oxygen from the ambient atmosphere. These effects should be present in our films where the protective surfactant coating has been rinsed away. The E^s_{11} transitions are affected more strongly than E^s_{22}.

Figure 4 shows the correlation plot between the optical absorbance, $a = -\log(T)$, at the wavelength of 775 nm and surface concentration of tubes forming the network. It demonstrates that the optical nonresonant

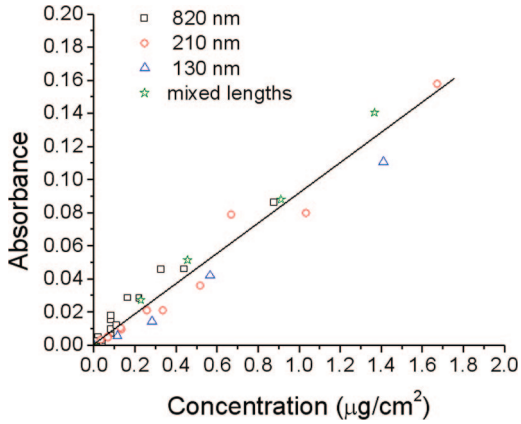

Figure 4. Optical absorbance at 775 nm as a function surface concentration for length-sorted SWCNTs.

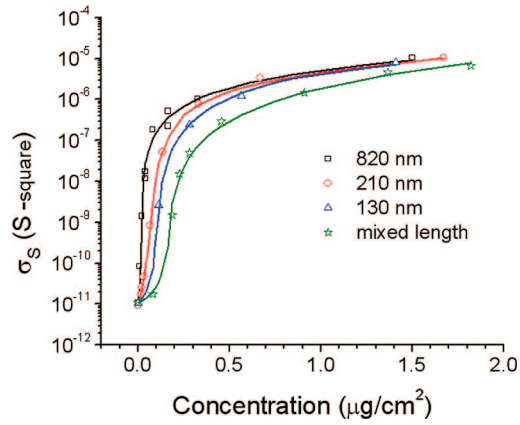

Figure 5. Conductivity as a function of surface concentration for length-sorted SWCNTs. The lines represent the fitted conductivities to the GEM percolation model.

absorption increases nearly linearly with concentration regardless of the tube length. A similar relationship holds for the films made of tubes of mixed length.

By changing the concentration of SWCNTs, the sheet conductivity (σ_s) of our 2D networks changes by 6 orders of magnitude, from 10^{-11} S-square to about 10^{-5} S-square as shown in Figure 5. Our σ_s values obtained for thicker SWCNT films are in the range of about 0.001 S-square, which is somewhat lower though comparable to the conductivity values reported for transparent electrode materials made of carbon nanotubes.[4,18,19] In contrast to optical absorption, which increases in linear proportion to the surface concentration, the sheet conductivity increases dramatically at low concentrations and saturates above a certain critical concentration. The overall character of the conductivity plots is characteristic of a percolation transition. Films made of mixed length tubes show the lowest conductivities, with the percolation transition taking place at higher concentration. With increasing tube length, the network conductivity increases and the percolation conditions for σ_s shift to lower concentrations. We also see that the crossover transition from the insulating to the conducting state occurs in a narrower concentration range. In the case of 820 nm length tubes, the characteristic step rise in conductivity takes place within a very narrow concentration range of about 0.008 μg/cm^2.

We determined the conductivity percolation concentration, x_c, and the critical percolation exponents, s and t, in relation to the tube length by analyzing the σ_s data in terms of the generalized effective medium theory (GEM):[12]

$$(1-x)\frac{\sigma_i^{1/s}-\sigma_s^{1/s}}{\sigma_i^{1/s}+A\sigma_s^{1/s}}+\varphi\frac{\sigma_a^{1/t}-\sigma_s^{1/t}}{\sigma_a^{1/s}+A\sigma_s^{1/t}}=0 \qquad (1)$$

where x is the tube concentration, A is a parameter related to the percolation concentration, $A = (1 - x_c)/x_c$, $\sigma_i \approx 10^{-11}$ S-square is the sheet conductivity of the in-

TABLE 1. Percolation Parameters of SWCNT Networks in Relation to the Tube Length

tube length (nm)	*s*	*t*	x_c (μg/cm^2)
820	1.25 ± 0.4	1.35 ± 0.1	0.018 ± 0.01
210	1.25 ± 0.5	1.38 ± 0.1	0.072 ± 0.07
130	1.2 ± 0.8	1.9 ± 0.1	0.095 ± 0.07
230 (mixed length)	0.8 ± 0.6	2.1 ± 0.1	0.15 ± 0.1

sulating matrix, and σ_a is the sheet conductivity of the network forming conducting additive (i.e., SWCNT). The strengths and limitations of GEM theory for describing the conductive properties of CNTs are discussed in our former paper,[13] and we apply the method without repeating this discussion here. From the asymptotic character of the experimental data at high SWCNT concentrations, we determined σ_a to be in the range of 5×10^{-5} S-square. Equation 1 fits our data well, and we then deduce x_c and the percolation exponents *t* and *s* using a nonlinear least-squares routine. The conductivity of the network in the high concentration limit is not equivalent to that of an isolated tube.[13] Rather, σ_a depends on the contact resistance between the CNTs[20−22] and other factors[4] that are not addressed in the simple GEM model. The critical percolation parameters obtained from eq 1 are summarized in Table 1 for the three different tube lengths. Interestingly, the universal percolation exponents *t* and *s* for the 820 nm and 210 nm tubes have similar values. These values are close to those theoretically expected for a large conducting 2D network,[23−26] where $s = t \approx 1.3$. Kholodenko and Freed[27] argue for the exact 2D exponent value, 23/18 ≈ 1.28. Thus, we find experimental evidence that our SWCNT networks can be described as nearly two-dimensional and that GEM percolation theory provides quantitative description of conductivity changes in these materials through the conductivity percolation transition. We note that the critical conductivity percolation concentration that we observe experimentally for the 820 nm tubes (x_c = 0.018 μg/cm^2) is one of the smallest reported to date.

The data in Table 1 indicate that the universal percolation exponents (*s* and *t*) obtained for networks made of the shorter tubes, and especially films formed with mixed length tubes, differ from values predicted for the 2D networks. Rather, they are found to be in accord with those predicted by GEM theory in 3D, $s \approx 0.8$ and $t \approx 2.0$. This indicates that an increasing fraction of SWCNT connections are being made in the third dimension in these short tube networks.[25,26,28]

The variation of the percolation threshold with the tube aspect ratio can be further understood on the basis of percolation and effective medium theory concepts. A polynomial expansion of the conductivity σ_s for a two-dimensional layer containing arbitrarily oriented particles of fixed and identical shape relative to an insulating layer without the particles is given by eq 2[29]

$$(\sigma_s / \sigma_i) = 1 + [\sigma]_\infty x + O(x^2) \quad (2)$$

where in 2D the leading virial coefficient $[\sigma]_\infty$ represents intrinsic conductivity of circular conducting discs.[30] Reference 29 provides results for numerous special cases and shows that $[\sigma]_\infty$ for arbitrary shaped particles can be generally related to the particle transfinite diameter. Accordingly, for an elliptic shaped particle having aspect ratio *L*, $[\sigma]_\infty$ is given by eq 3:

$$[\sigma]_\infty = (1 + L)^2 / 2L \quad (3)$$

The percolation transition concentration x_c can be estimated based on the conditions that the leading correction to the conductivity becomes on the order, $[\sigma]_\infty x \approx 0(1)$, a Ginzburg criterion.[30,31] This condition, along with eq 3, implies the general scaling relation for the conductivity percolation concentration in 2D for slender particles is

$$x_c(\text{slender particle}) \sim 1 / L \quad (4)$$

Equation 4 suggests that, in networks exhibiting 2D percolation transition, increasing the CNT length by a factor of 820 nm/210 nm = 3.9 should decrease the corresponding percolation threshold x_c by a similar factor. Table 1 indicates that x_c is indeed reduced by a factor of 4.0 in our buckypaper films, in quantitative agreement with eq 4. In a similar fashion, x_c can be predicted for particles having arbitrary shape.[31,32] Thus, we find that the optical characteristics of the length fractionated SWCNTs are distinct from unsorted polydisperse SWCNTs.

Projecting the percolation conductivity plot (Figure 5) onto the linear plot of optical absorbance (Figure 4) indicates that the direct correlation between the off-resonant π-plasmon absorbance and the network conductivity will obey the percolation model (eq 1). In particular, primarily the universal percolation exponents will govern the optical absorbance of thin SWCNT films. This result is quantitatively different and more universal than that adopted for SWCNTs based on the optical properties of thin metallic films below the diffraction limit.[5,33] The characteristic electronic transitions giving rise to chirality specific absorption bands are magnified in longer tubes. The longer fractionated tubes are both more transparent and conducting at the same surface coverage. The universal percolation exponents obtained for the long length tubes conform well to the predictions of GEM percolation theory in 2D. Again, the critical conductivity percolation concentration of 0.018 μg/cm^2 in these 2D networks is the lowest reported to

date. Short and mixed length tubes (Table 1) form networks for which the universal percolation exponents are consistent with the 3D percolation model. These observations indicate that considerable control on the conductivity and optical properties can be obtained by adjusting SWCNT length, concentration, and polydispersity. The GEM percolation theory provides a convenient framework for describing and engineering these changes for nanotechnology applications, exploiting these novel materials.

EXPERIMENTAL METHODS

Single-walled carbon nanotubes, SWCNTs, grown by the cobalt−molybdenum catalyst (CoMoCat) process, were purchased from Southwest Nanotechnologies, Inc. (S-P95-02 grade, batch NI6-A001).[1] The SWCNTs were dispersed at 1 mg soot/mL in a 2% mass fraction of sodium deoxycholate (DOC) aqueous surfactant solution *via* sonication (tip sonicator, 0.64 cm, Thomas Scientific) for 1.5 h in an ice water bath at 1 W/mL applied power. Post-sonication purification was performed by centrifugation at an acceleration of 21 000 × 9.81 m/s^2 (21 × 10^3 G) for 2 h to pellet the non-SWCNT carbonaceous and catalyst impurities. The collected supernatant contained primarily individually dispersed SWCNTs. In order to separate the purified SWCNTs by length, we used a dense liquid centrifugation method.[11] Density layers were formed directly in the centrifuge tubes by layering appropriate concentrations of iodixanol (Sigma Aldrich Inc.)−deoxycholate solutions such that the density of the surrounding medium ($\Delta\rho_{layer}$) is larger than that of the tubes ($\Delta\rho_{layer} \gg \Delta\rho_{SWNT}$) in all layers. The difference in scaling with length of the hydrodynamic and buoyancy forces on the individual SWCNTs was then used to generate length separation under high acceleration. Separation was performed in a SW-32 rotor using a Beckman Coulter L80 XP ultracentrifuge at 1445 rd/s for 70 h. Typically, 16 individual fractions were collected after centrifuging, by hand-pipetting in 1.5 mL increments from the top. From these, we selected three fractions having mean tube lengths of 820, 210, and 130 nm, respectively. After the length separation, the SWNT mass fraction improves considerably to better than 95%. We also used the purified unsorted SWCNT suspension, which had a mean tube length of ≈220 nm and a standard deviation of ≈20. However, the length distribution of this sample is approximately a log-normal and contains a broader distribution of tubes of varying length (mixed length fraction). This was our model polydisperse sample. Length fractions were dialyzed after separation against 0.8% DOC solution to remove the remaining iodixanol and to reduce the total surfactant concentration.

The average length (L) of the fractionated SWCNTs was characterized by atomic force microscopy (AFM) and transmission electron microscopy (TEM) and was verified by the intensity of the electronic absorption peak at 984 nm on the NIR spectrum.[11] The combined relative uncertainty of L mean value was approximately 10%, while each fraction distribution had a standard deviation value of about 20%.

The optical absorbance spectra of the SWCNT aqueous suspensions in the UV−vis−NIR range (300−1800) nm were obtained using a Perkin-Elmer Lambda 950 UV−vis−NIR spectrophotometer.

Fractionated SWCNTs were then deposited on the surface of a porous cellulose ester membrane, diameter of 47 mm, with 0.05 μm diameter pore size (Millipore), *via* a vacuum filtration process.[2] The active area of the membrane surface was 10.2 cm^2 (diameter 36 mm). A mixture of isopropanol and deionized water (1:4) by volume was used to "condition" the membranes and to rinse away the deoxycholate surfactant. The concentration tubes in fractionated suspensions were typically between 0.05 and 0.1 mg/mL, determined by weighing the tube deposit on a microbalance after dialyzing and evaporating a fixed volume of fractionated suspension. The networks' surface density was controlled by varying the volume of the fractionated suspension using a micropipette (Oxford Benchmate), then diluting the suspension with DI water to obtain 2 mL of dilute suspension. The deposited SWCNTs from the dilute suspension formed a random network on the surface of the membrane. The samples were then dried at 50 °C for 24 h under nitrogen atmosphere. The surface density of these networks was in the range of 0.01 to 2.0 μg/cm^2 with the combined relative uncertainty of 30%.

The optical characteristics of the SWCNT networks were determined by measuring the diffuse optical reflectance in the wavelength range of 300−1800 nm, using a diffuse reflectance accessory kit for the Lambda 950. The reflectance spectra were normalized to the reflectivity of the filter membrane without SWCNTs, which we used as a nonabsorbing reference. Thus, the spectra primarily represent the absorbance of the conducting SWCNT film.

The scanning electron microscopy images of the deposited SWCNT networks were obtained using a Hitachi S4700 field emission scanning electron microscope.

To measure the electrical characteristics of the network films, an interdigitated gold electrode pattern was deposited directly on top of the SWCNT network through a shadow mask. Electrical measurements were analyzed in terms of complex impedance, yielding the impedance magnitude ($|Z^*|$) and the corresponding phase angle (θ) over the frequency range of 40−10 MHz by using a four-terminal fixture attached to an Agilent 4294A precision impedance analyzer.[13] The impedance analyzer was calibrated with a standard extension adapter to short, load, and open standards. The real part (σ') of the complex sheet (surface) conductivity was determined from the measured impedance normalized by the geometry of the electrode pattern

$$\sigma' = \left[1 / \left(\left|Z^*\right| \cos(\theta)\right)\right](1 / d)$$

in units of $(\Omega/\text{square})^{-1}$ or Siemens-square (S-square). Here, l is the total length of the finger electrodes, and d is the distance between the fingers. In our measurements, $l = 9$ cm and $d = 800$ μm. The thickness of the deposited gold electrodes was about 0.1 μm. The lowest measurable sheet conductivity in our system was $\sigma' \approx 5 \times 10^{-12}$ S-square at 100 Hz. The sheet conductivity of dried blank membrane substrates, without carbon nanotubes, was typically below 10^{-11} S-square at 100 Hz. The combined relative experimental uncertainty of the measured conductivity magnitude was within 4%, while the experimental uncertainty of the phase angle measurements was about ±0.5°. The sheet conductivity σ' of our SWCNT films is frequency dependent but at the lowest frequencies exhibits a plateau that persists up to crossover frequency of ω_s. Throughout our paper, we denote this frequency independent real conductivity $\sigma'(\omega \to 0, \theta \approx 0)$ as σ_s. At higher frequencies, $\omega > \omega_s$, we observe that σ' increases with increasing frequency according to power law, $\sigma' \sim \omega^n$, which is commonly described as a "universal" property of disordered solids and applicable to a broad range of semiconducting materials, conductor−dielectric mixtures, and composites.[7,13]

Note: Certain equipment, instruments, or materials are identified in this paper in order to adequately specify the experimental details. Such identification does not imply recommendation by the National Institute of Standards and Technology nor does it imply the materials are necessarily the best available for the purpose.

Acknowledgment. We thank Thuy Chastek for help in SEM imaging. W.L. acknowledges support from the NIST Summer Undergraduate Research Fellowship Program.

REFERENCES AND NOTES

1. Unalan, H. E.; Fanchini, G.; Kanwal, A.; Du Pasquier, A.; Chhowalla, M. Design Criteria for Transparent Single-Wall Carbon Nanotube Thin-Film Transistors. *Nano Lett.* **2006**, *6*, 677–682.
2. Wu, Z. C.; Chen, Z. H.; Du, X.; Logan, J. M.; Sippel, J.; Nikolou, M.; Kamaras, K.; Reynolds, J. R.; Tanner, D. B.; Hebard, A. F.; et al. Transparent, Conductive Carbon Nanotube Films. *Science* **2004**, *305*, 1273–1276.
3. Abraham, J.; Philip, B.; Witchurch, A.; Varadan, V.; Reddy, C. C. A Compact Wireless Gas Sensor Using a Carbon Nanotube/PMMA Thin Film Chemiresistor. *Smart Mater. Struct.* **2004**, *13*, 1045–1049.
4. Blackburn, J. L.; Barnes, T. M.; Beard, M. C.; Kim, Y. H.; Tenent, R. C.; McDonald, J.; To, B.; Coutts, T. J.; Heben, M. J. Transparent Conductive Single-Walled Carbon Nanotube Networks with Precisely Tunable Ratios of Semiconducting and Metallic Nanotubes. *ACS Nano* **2008**, *2*, 1266–1274.
5. Green, A. A.; Hersam, M. C. Colored Semitransparent Conductive Coatings Consisting of Monodisperse Metallic Single-Walled Carbon Nanotubes. *Nano Lett.* **2008**, *14*, 1417–1422.
6. Kumar, S.; Murthy, J. Y.; Alam, M. A. Percolating Conduction in Finite Nanotube Networks. *Phys. Rev. Lett.* **2005**, *95*, 066802-1–066802-4.
7. Li, J.; Ma, P. C.; Chow, W. S.; To, C. K.; Tang, B. Z.; Kim, J. K. Correlations between Percolation Threshold, Dispersion State, and Aspect Ratio of Carbon Nanotubes. *Adv. Funct. Mater.* **2007**, *17*, 3207–3215.
8. Kacabas, C.; Pimparkar, N.; Yesilyurt, O.; Kang, S. J.; Alam, M. A.; Rogers, J. A. Experimental and Theoretical Studies of Transport through Large Scale, Partially Aligned Arrays of Single-Walled Carbon Nanotubes in Thin Film Type Transistors. *Nano Lett.* **2007**, *7*, 1195–1202.
9. Behnam, A.; Guo, J.; Ural, A. J. Effects of Nanotube Alignment and Measurement Direction on Percolation Resistivity in Single-Walled Carbon Nanotube Films. *Appl. Phys.* **2007**, *102*, 044313-1–044313-7.
10. Rinzler, A. G.; Liu, J.; Nikolaev, P.; Huffman, C. B.; Rodriguez-Macias, F. J.; Boul, P. J.; Lu, A. J.; Heymann, D.; Colbert, D. T.; Lee, R. S.; et al. Large-Scale Purification of Single-Wall Carbon Nanotubes: Process, Product, and Characterization. *Appl. Phys. A: Mater. Sci. Process.* **1998**, *67*, 29–37.
11. Fagan, J. A.; Becker, M. L.; Chun, J.; Hobbie, E. K. Length Fractionation of Carbon Nanotubes Using Centrifugation. *Adv. Mater.* **2008**, *20*, 1609–1613.
12. McLachlan, D. S.; Heiss, W. D.; Chiteme, C.; Wu, J. Analytic Scaling Functions Applicable to Dispersion Measurements in Percolative Metal-Insulator Systems. *Phys. Rev. B* **1998**, *58*, 13558–13564.
13. Obrzut, J.; Douglas, J. F.; Kharchenko, S. B.; Migler, K. B. Shear-Induced Conductor-Insulator Transition in Melt-Mixed Polypropylene-Carbon Nanotube Dispersions. *Phys. Rev. B* **2007**, *76*, 195420-1–195420-9.
14. Weisman, R. B.; Bachilo, S. M. Dependence of Optical Transition Energies on Structure for Single-Walled Carbon Nanotubes in Aqueous Suspension: An Empirical Kataura Plot. *Nano Lett.* **2003**, *3*, 1235–1238.
15. Louie, S. G. Electronic Properties, Junctions, and Defects in Carbon Nanotubes. In *Carbon Nanotubes: Synthesis, Structure, Properties, and Applications*; Dresselhaus, M. S., Dresselhaus, G., Avouris, P., Eds.; Topics in Applied Physics: Springer, NY, 2000; Vol. 80; pp 113−143.
16. Jorio, A. P.; Ribeiro, H. B.; Fantini, C.; Souza, M.; Vieira, J. P. M.; Furtado, C. A.; Jiang, J.; Saito, R.; Balzano, L.; Resasco, D. E.; et al. Quantifying Carbon-Nanotube Species with Resonance Raman Scattering. *Phys. Rev. B* **2008**, *72*, 075207-1–075207-5.
17. Yanagi, K.; Miyata, Y.; Kataura, H. Optical and Conductive Characteristics of Metallic Single-Wall Carbon Nanotubes with Three Basic Colors; Cyan, Magenta, and Yellow. *Appl. Phys. Express* **2008**, *1*, 034003-1–034003-3.
18. Pelota, J.; Weeks, C.; Levitsky, I. A.; Britz, D. A.; Glatkowski, P.; Trotier, M.; Huang, T. Carbon Nanotube Transparent Electrodes for Flexible Displays. *Inf. Display* **2007**, *2*, 2–5.
19. Rowell, M. W.; Topinka, M. A.; McGehee, M. Organic Solar Cells with Carbon Nanotube Network Electrodes. *Appl. Phys. Lett.* **2006**, *88*, 233506-1–233506-3.
20. Fuhrer, M. S.; Nygard, J.; Shih, L.; Forero, M.; Yoon, Y. G.; Mazzoni, M. S. C.; Choi, H. J.; Ihm, J.; Louie, S. G.; Zettl, A.; et al. Crossed Nanotube Junctions. *Science* **2000**, *288*, 494–497.
21. Obrzut, J.; Migler, K.; Dong, L. F.; Jiao, J. *Frontiers of Characterization and Metrology for Nanoelectronics*; APS Conf. Proceedings, 2007; Vol. 931, pp 483−485.
22. Derirda, B.; Vannimenus, J. A Transfer-Matrix Approach to Random Resistor Networks. *J. Phys. A.* **1982**, *15*, L557–L564.
23. Clerc, J. P.; Giraud, G.; Laugier, J. M.; Luck, J. M. The Electrical Conductivity of Binary Disordered Systems, Percolation Clusters, Fractals and Related Models. *Adv. Phys.* **1990**, *39*, 191–309.
24. Frank, D. J.; Lobb, C. J. Highly Efficient Algorithm for Percolative Transport Studies in Two Dimensions. *Phys. Rev. B* **1988**, *37*, 302–307.
25. Laugier, J. M.; Clerc, J. P.; Giraud, G.; Luck, J. M. AC Properties of 2D Percolation Networks: A Transfer Matrix Approach. *J. Phys. A: Math. Gen.* **1986**, *19*, 3153–3164.
26. Lajkó, P.; Turban, L. Percolation and Conduction in Restricted Geometries. *J. Phys. A: Math. Gen.* **2000**, *33*, 1683–1692.
27. Kholodenko, A. L.; Freed, K. F. Diffusion in Random Media as a Problem of Interacting Bose and Fermi Fields. *J. Phys. A: Math. Gen.* **1984**, *17*, L55–L59.
28. Stauffer, D. *Introduction to Percolation Theory*; Tayler & Francis Ltd.: London and Philadelphia, 1985.
29. Douglas, J. F.; Garboczi, E. J. Intrinsic Viscosity and the Polarizability of Particles Having a Wide Range of Shapes. *Adv. Chem. Phys.* **1995**, *91*, 85–153.
30. Dudowicz, J.; Lifschitz, M.; Freed, K. F.; Douglas, J. How Far Is Far from Critical Point in Polymer Blends? Lattice Cluster Theory Computations for Structured Monomer, Compressible Systems. *J. Chem. Phys.* **1993**, *99*, 4804–4820.
31. Bicerano, J.; Douglas, J. F.; Brune, D. A. Model for the Viscosity of Particle Dispersions. *J. Macromol. Sci., Rev Marcomol. Chem. Phys.* **1999**, *C39*, 561–642.
32. Garboczi, E. J.; Snyder, K. A.; Douglas, J. F.; Thorpe, M. F. Geometrical Percolation of Overlapping Ellipsoids. *Phys. Rev. E* **1995**, *52*, 819–828.
33. Zhou, Y.; Hu, L.; Gruner, G. A Method of Printing Carbon Nanotube Thin Films. *Appl. Phys. Lett.* **2006**, *88*, 123109-1–123109-3.